LARGE-EDDY SIMULATION OF THE TURBULENT FLOW IN DUCTS : A STUDY OF HEATING AND CURVATURE EFFECTS

Hébrard Jérôme & Métais Olivier
L.E.G.I./Institut de Mécanique de Grenoble
B.P. 53, 38041 Grenoble Cedex 09, France
hebrard@hmg.inpg.fr

Salinas-Vasquez Martin
Instituto de Ingenieria, UNAM, MEXICO
msv@quetzal.iingen.unam.mx

ABSTRACT

We first study the spatial development of turbulent flow inside a straight duct of square section : heating with a constant temperature is applied suddenly at a given downstream location of the duct. The downstream development of the thermal boundary layer is then studied and compared with the case of a fully developed flow within a heated duct. We investigate the influence of the heating on the flow structures such as low-speed streaks, ejections etc .. The use of curvilinear coordinates allows us to consider duct with more geometries and curvature effects are then studied. The case of a S-shape duct is considered exhibiting both convex and concave curvatures. We assist to the formation of Görtler type vortices and the influence of the heating is investigated.

INTRODUCTION

For numerous engineering applications, it is necessary to reach a deeper understanding and a better prediction of the heat exchanges between a heated wall and the surrounding turbulent flow. Among these applications, one may quote the improvement of the performances of the heat exchangers, of the cooling of the rocket engines, etc ... In previous works, we have successfully applied the Large-Eddy Simulation (LES) technique based on the structure function subgrid-scale model (see Lesieur and Métais (1996)) to the study of both the statistitical characteristics and the instantaneous three-dimensional structures in the turbulent flow through a heated duct (see Salinas-Vazquez and Métais (2002) and (2001)) at $Mach = 0.5$. Salinas-Vazquez and Métais (2002) considered square ducts with a prescribed temperature at each wall. When heating was applied, the temperature imposed at the heated wall was higher than the temperature of the other three walls. With this type of thermal boundary conditions, simple periodic boundary conditions can be used in the streamwise direction. However, in several industrial devices involving heated boundary layers, a given heat-flux is actually imposed at the heated wall and the turbulent flow can no longer be assumed periodic in the streamwise direction ought to the continuous energy increase along this direction. One has then to deal with spatially developing turbulent flows which require a more complex prescription of inflow and outflow boundary conditions (see e.g. Poinsot and Lele, 1992). In a first part, we investigate, through LES with the structure function subgrid-scale model the spatial development of a thermal boundary layer in a straight duct with a square section : the temperature of one of the walls is suddenly increased from $T_h/T_w = 1.0$ to $T_h/T_w = 2.5$. Results are compared with the case of a fully developed flow (Salinas-Vasquez and Métais, 2002). Through the use of curvilinear coordinates we investigate, in a second part, the effects of curvature. The S-shape duct is considered since it presents the interesting feature of having a convex-concave wall on one of its side and of a concave-convex wall on the other side.

NUMERICAL CONFIGURATION

In the simulations, we use ducts of square section. Preliminary results for the spatially developing flow in a straight duct were obtained by Salinas-Vasquez and Métais (2001). We first reconsider Salinas-Vasquez and Métais' LES study but with a straight duct of double length. We use the same numerical code as Salinas-Vasquez and Métais (2001) solving the three-dimensional compressible Navier-Stokes equations. The system of equations in generalized coordinates is solved by mean of a compact scheme extension of the McCormack scheme, second order in time and fourth in space proposed by Kennedy and Carpenter (1997). The Mach number is taken equal to 0.5 and the Reynolds number based on the bulk velocity to 6000. Fully turbulent inlet boundary conditions are provided at each time step by a LES of a duct with all its walls at the imposed temperature T_w. This longitudinally periodic duct (called temporal duct) is linked to the spatially growing duct through the characteristics boundary conditions proposed by Poinsot & Lele (1992) (Figure 1). The size of the computational domain is taken equal to $31Dh * Dh * Dh$ (Dh is the duct hydraulic diameter) for the spatial duct and $6.4Dh * Dh * Dh$ for the temporal duct with the first length corresponding with the streamwise direction and the other two with the two transverse directions. The corresponding number of grid points are respectively $318 * 50 * 50$ and $64 * 50 * 50$. A similar procedure is then used to generate the turbulent inflow conditions for a S-shape duct (see figure 2). In that case, the size of the domain is taken equal to $15Dh * Dh * Dh$. The corresponding number of grid points are respectively $160 * 50 * 50$ in the curvilinear coordinates s,n and z ; s follows the concave-convex wall, it will be assumed that $n/Dh = 0$ on this wall, and z is in conformity with the right-hand rule.

RESULTS

Straight duct

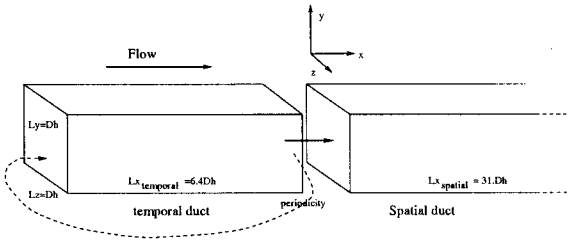

Figure 1: numerical configuration

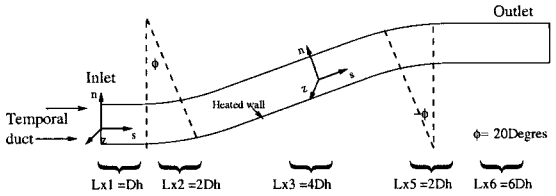

Figure 2: S-shape duct configuration

To obtain the development of a thermal boundary layer, the temperature of one of the walls is suddenly increased from $T_h/T_w = 1.0$ to $T_h/T_w = 2.5$. Figure 3 shows the u'_{rms} and w'_{rms} profiles as a function of the distance y from the heated wall and at two locations from the lateral wall, $z/D_h = 0.5$ corresponding to the duct middle plane. The profiles are normalized by the bulk velocity. A comparison is made with the fully developed duct computation by Salinas-Vasquez and Métais (2002), both in the heated case ($\triangle$) $T_h/T_w = 2.5$ and in the non-heated case ($\square$). To observe the longitudinal evolution of the flow, profiles for seven different x-planes $x/D_h = 0.9$, $x/D_h = 10$, $x/D_h = 17$, $x/D_h = 22$, $x/D_h = 26$, $x/D_h = 30$ and $x/D_h = 31$ are presented. The results for the spatially developing case exhibit similar features than the fully developed heated case (Salinas-Vasquez and Métais, 2002). The increase of the temperature induces an enhancement of the viscosity. Consequently, the u'_{rms} and w'_{rms} are progressively reduced near the heated wall has we go downstream. The low-speed and high-speed streaks are also modified by the heating. At $z/D_h = 0.5$, the maximal u'_{rms} value is progressively shifted away from the heated wall indicating an enhancement of the mean size of the near wall turbulent structures.

The comparison between the spatially developing and the fully developed heated cases shows, in the former case, lower turbulent intensities mainly for $z/D_h = 0.5$ and $y/D_h > 0.15$. In the fully-developed configuration, strong ejections generated around the middle plane of the hot wall induce indeed a significant increase of the turbulence activity for $y/D_h > 0.15$ (see Salinas-Vasquez and Métais, 2002). The strong ejections are still not fully developed in the spatial duct by the end of the duct although the rms profiles are similar in shape to the fully developed case. The fact that the ejections are not fully developed in the spatial can also be observed from the $\langle u'v' \rangle$ profiles, figure 4. It is well known that the ejections are the principal source for this Reynolds stress component. In the fully-developed simulations, the profiles display an enhancement of $\langle u'v' \rangle$ at $z/D_h = 0.5$ and for $y/D_h > 0.15$, and an increase of the ejection activity (Salinas-Vasquez and Métais, 2002). As we go further and further donwnstream, the maximum in the profile is shifted away from the heated wall showing an increase in the size of the ejections. The amplitude of the maximum is however not increased indicating that the viscosity enhancement plays damps the fluctuations near the heated wall. Another way to characterize the size of the ejections is by looking at the temperature and temperature fluctuations profiles (see figure 5). The mean temperature decreases rapidly from T_h at the heated wall to a value close to T_w, temperature at the opposite wall. As compared to the fully-developed case, the temperature gradient is much stronger in the spatial case : this is directly linked with the reduced size of the ejections which do not mix the hot temperature as efficiently as when the turbulence is fully developed.

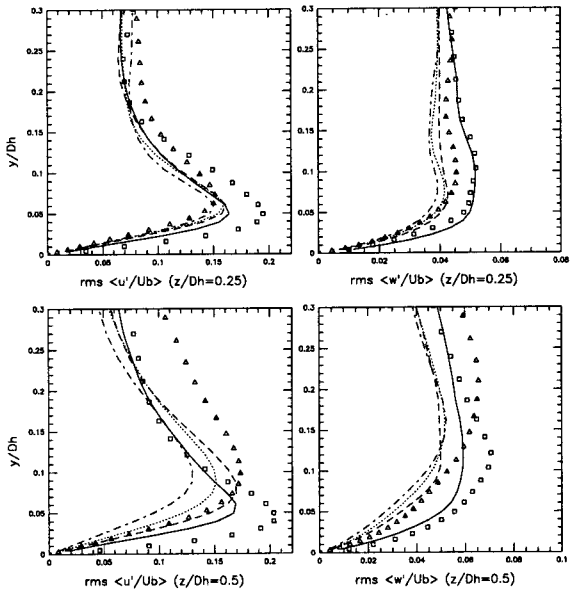

Figure 3: Zoom on u'_{rms} and w'_{rms} profiles close the hot wall as a function of the distance y from the wall and at a fixed distance $z/D_h = 0.5$ and $z/D_h = 0.25$ from the lateral wall. Temporal duct, ($\triangle$); isothermal ducti, ($\square$). Spatial ducts for different distances from the inlet: $x/D_h = 10$, (—-); $x/D_h = 22$, (- -) ; $x/D_h = 26$, (- - -) ; $x/D_h = 31$, (- - -); Values are normalized by the local bulk velocity.

This strong temperature gradient induce an important production for T'_{rms}. T'_{rms} profiles display peaks in the region of maximal temperature gradient. It is interesting to note that the stronger mean-temperature gradients induce a higher level of temperature fluctuations near the heated wall. The opposite is observed in the outer region. The mean temperature gradient is less important at $z/D_H = 0.5$ than $z/D_H = 0.25$ showing that the ejections are located around the duct middle plane. This is confirm by the T'_{rms} profiles whose peaks, in the middle plane, are clearly shifted upwards in the downstream part of the duct.

As shown by Salinas-Vasquez and Métais (2002), the heating has a significant influence on the topology of the turbulent structures. The viscosity increase induces a global enhancement of the near wall structures such as the low- and high-speed streaks and the associated ejections. The size of the ejections becomes such that they concentrate near the middle plane of the duct. Similar changes are observed in the spatially growing duct. The advantage of this simulation is the ability to visualize the progressive change of the flow structures near the heated wall. The increase in size of the streaky structures principally due to the enhancement of the viscous thickness is clearly observed.

Figure 6 shows a view looking at the heated wall of the fluctuating fields for the temperature and the streamwise velocity close to the heated wall at $y/D_h = 0.01$. Positive streamwise fluctuations correspond to sweeps towards

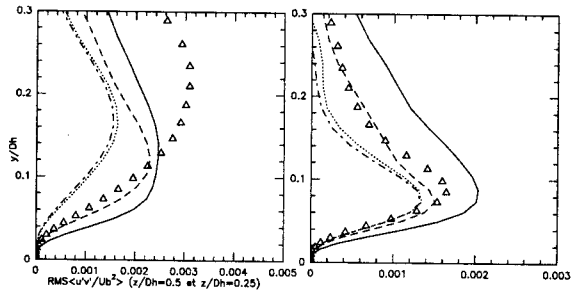

Figure 4: Zoom on $\langle u'v' \rangle$ profiles close the hot wall as a function of the distance y from the wall and at a fixed distance $z/D_h = 0.5$ and $z/D_h = 0.25$ from the lateral wall. Temporal duct, ($\triangle$); isothermal duct, ($\square$). Spatial duct for different distances from the inlet: $x/D_h = 10$, (—-); $x/D_h = 22$, (- -) ; $x/D_h = 26$, (- - -) ; $x/D_h = 31$, (- - -); Values are normalized by the local bulk velocity.

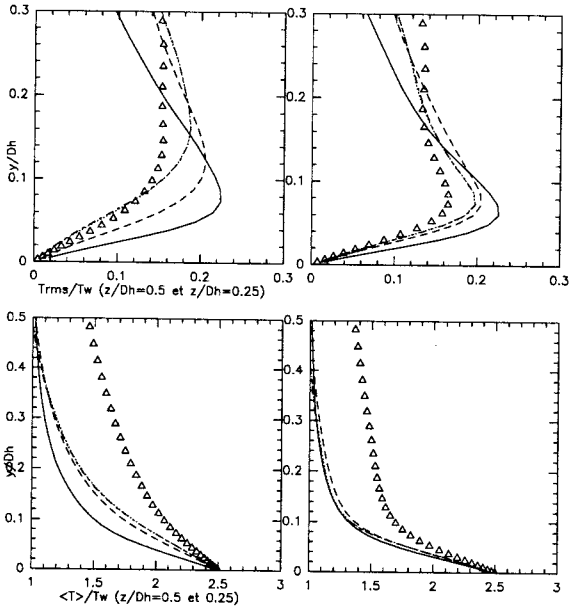

Figure 5: Zoom on T/T_w and $Trms/T_w$ profiles close the hot wall as a function of the distance y from the wall and at a fixed distance $z/D_h = 0.5$ and $z/D_h = 0.25$ from the lateral wall. Temporal duct, ($\triangle$); Spatial duct for different distances from the inlet: $x/D_h = 10$, (—-); $x/D_h = 22$, (- -) ; $x/D_h = 26$, (- - -) ; $x/D_h = 31$, (- - -); Values are normalized by the fixed isothermal wall temperature.

the wall and negative streamwise fluctuations are associated with ejections. The former correspond to cold fluid transported towards the wall (negative temperature fluctuations) and the latter to hot fluid ejected into the colder outer region (positive temperature fluctuations). Near the inlet, the streaks display their characteristic long and narrow shape. From $x/D_h \approx 6.0$ the streaks are longer and wider than in the inlet region. Eventually, the streaks are so wide and that two or three streaks are visible at the end of the duct. It is now well recognized that the Q criterion based upon the second invariant of the velocity derivative tensor is a good way to identify the coherent structures (Hunt et al., 1988), (Dubief and Delcayre, 2000). Turbulent structure, identified with the positive Q isosurfaces, are very numerous at the inlet, but their number decreases in function of the streamwise direction. They concentrate around the middle wall plane and their longitudinal length is higher close to the outlet. The flow structures observed between $x/D_h = 12$ and 30 in the vicinity of the middle wall plane (bottom of the figure 6) are typical examples of turbulent structures found in the fully-developed heated duct. Figure 7 shows the instantaneous temperature field contours and the instantaneous transversal velocity vectors at four different x-planes. The evolution of the big ejection is strongly linked to the increase of the instantaneous secondary flow size. Close to the inlet region, the secondary flows pattern near the hot wall is similar to the one on the other three walls. Small ejections are observed on the heated wall. However close to the outlet, a big structure forms which ejects hot fluid from the heated wall.

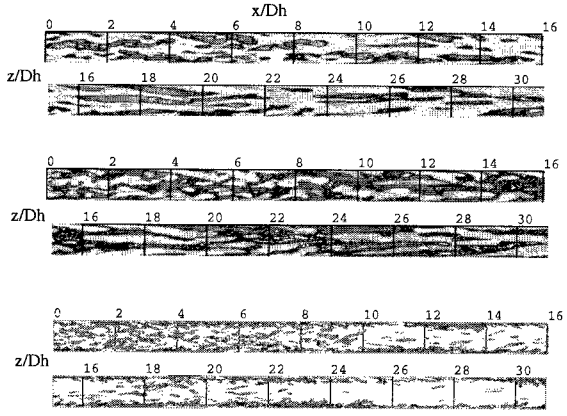

Figure 6: Heated duct turbulent structures. **top** Fluctuant streamwise velocity near the hot wall. **middle** Fluctuant temperature near the hot wall. **bottom** Instantaneous Q isosurfaces Q=0.5 $(U_b/D_h)^2$ on the hot wall.

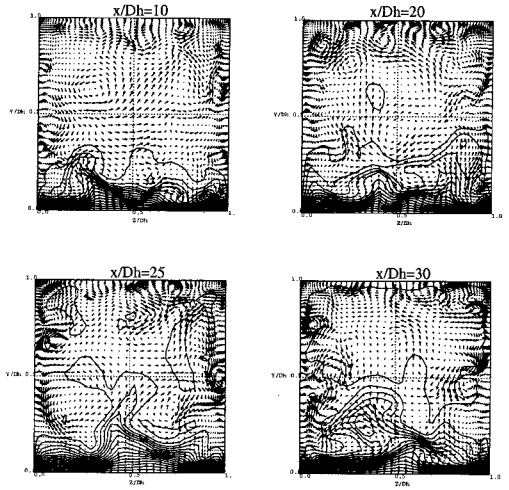

Figure 7: Instantaneous temperature and transversal velocity vector fields for $x/D_h = 10$, 20, 25 and 30.

S-shape duct

The laboratory experiments by (Chebbi et al., 1998) (bruns et al., 1999) and the numerical studies by (Jongen et al., 1998) have shown that the flow downstream of a concave-convex wall requires a longer length to recover the statistics of the straight duct than the flow downstream of a convex-concave wall. It is well known that square ducts are characterized by the presence of mean secondary flows which are perpendicular to the mean flow direction. In the case of the straight duct, these have a weak amplitude

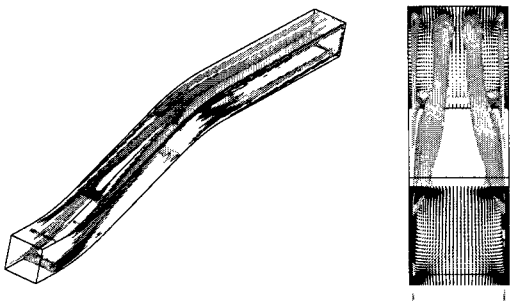

Figure 8: Mean visualization of the Dean vortices in the S-shape duct.

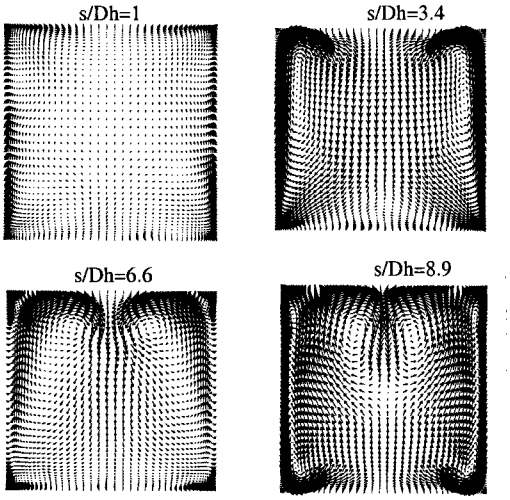

Figure 9: Isothermal S-shape duct : Visualization of the mean secondary flows.

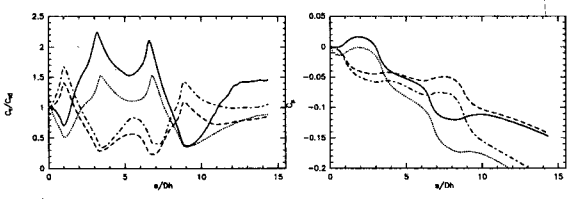

Figure 10: Skin friction coefficient normalized by its value at the inlet (left) ; coefficient of pressure (right). isothermal S-shape duct : (——) $n/D_h = 0$ (concave/convex wall); (– –) $n/D_h = 1$ (convex/concave wall); Heated S-shape duct : (- - - -) $n/D_h = 0$; (– - –) $n/D_h = 1$;

of the order of $1 - 2\%$ of the bulk velocity (see Salinas-Vasquez and Métais, 2002). In the case of the curved duct with sufficient curvature, the centrifugal instability may take place leading to a significant enhancement of the secondary flows. For our duct computation, the visualization of the mean longitudinal vorticity clearly shows the formation of two longitudinal contra-rotative vortices corresponding to the so-called Görtler vortices. These are associated with an amplitude of the secondary flow of the order of 30% of the bulk velocity (see figure 8). On figure 9, the enhancement on the vortices begins in the first curvature section ($s/D_h = 1$) and continue until the outlet, and a pair of two vortices stays closed the convex-concave wall. Both curvature sections seem to have a very significative effect on secondary flow. These Görtler vortices carry the fluid from the walls to the core of the duct. Figure 10 shows the skin friction

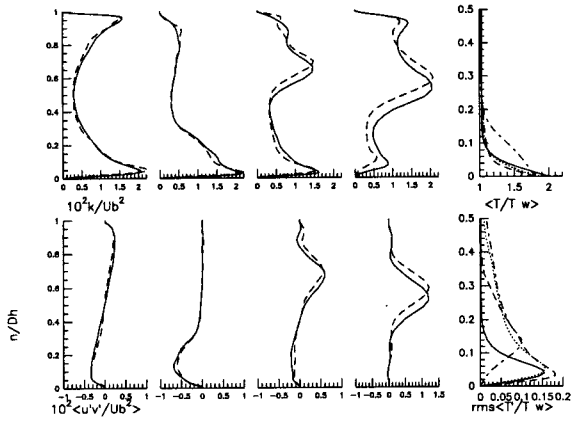

Figure 11: (Left) Profiles of the turbulent kinetic energy and Reynolds shear stress as a function of the distance n from the wall and at a fixed distance $z/D_h = 0.5$ from the lateral wall. Isothermal S-shape duct (——) ; Heated S-shape duct (– – –) ; for different distances from the inlet: $s/D_h = 1$; $s/D_h = 3.4$; $s/D_h = 6.7$; $s/D_h = 8.9$ Values are normalized by the local bulk velocity. (Right) T/T_w and $Trms/T_w$ profiles close the hot wall as a function of the distance n from the wall and at a fixed distance $z/D_h = 0.5$ from the lateral wall. Heated S-shape duct for different distances from the inlet: $s/D_h = 1$, (—-); $s/D_h = 3.4$, (– –) ; $s/D_h = 6.7$, (- - -) ; $s/D_h = 8.9$, (– - –); Values are normalized by the fixed isothermal wall temperature.

coefficient

$$c_f = \frac{\langle \tau_w(\vec{x}) \rangle}{1/2 {U_b}^2 \rho_b} \tag{1}$$

and the coefficient of pressure

$$c_p = \frac{\langle P(\vec{x}) - P_o(\vec{x}) \rangle}{1/2 {U_b}^2 \rho_b} \tag{2}$$

Near the inlet ($s/D_h < 5$), the skin friction is enhanced along the concave wall ($n/D_h = 0$) (figure 10). Conversely, the skin friction is reduced on the convex wall : there exists a normal pressure gradient to the walls which drives the flow from the concave wall ($n/D_h = 0$) to the convex wall ($n/D_h = 1$) (on figure 10, between $s/D_h = 1$ and 3.4 corresponding to the first curvature, the pressure coefficient on the concave wall is higher than on the convex one). From the middle of the duct to the outlet, ($s/D_h > 6$), the skin friction enhanced still long the concave wall which is now $n/D_h = 1$. The normal pressure gradient is in the opposite direction and drives the vortices towards the core of the duct. The flow acceleration near the start of the first curvature close the convex wall is linked with the positive longitudinal pressure gradient, the opposite phenomenum takes place near the concave wall. These pressure gradients are directly associated with the centrifugal force. The destabilizing and stabilizing effects of the concave and convex walls can be seen on the turbulent kinetic energy and Reynolds shear stress profiles. Figure 11 shows the profiles of $k = \frac{1}{2}(\langle u'^2 \rangle + \langle v'^2 \rangle + \langle w'^2 \rangle)$ and $\langle u'v' \rangle$ at the start and at the end of each curvature and in t he duct middle plane $z/D_h = 0.5$. In the first bend of the duct, both k and $\langle u'v' \rangle$ are clearly enhanced in magnitude near the concave wall ($n/D_h = 0$) as compared with the convex wall ($n/D_h = 1$). In the second bend, the same observation can be made but now the concave wall corresponds to $n/D_h = 1$. The maxima of k and $\langle u'v' \rangle$ increase by about 10% on the concave wall of the first bend and about 20% in the second bend. Conversely, the turbulence intensity is clearly reduced near the convex wall showing a stabilization mechanism. We can

observe the formation of a two layers structure between the second curvature and the outlet of the duct. The turbulent kinetic energy loose about 50 % of its value and changes significaly its profile. The turbulent activity is driven to the core near the outlet of the duct. The negative normal pressure gradient is in question is this displacement of activity.

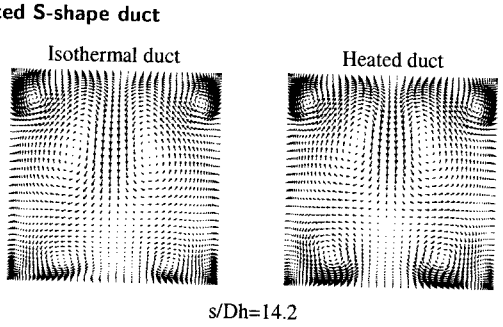

Figure 12: Comparison between the isothermal and the heated S-shape duct : Visualization of the mean secondary flows at the outlet of the duct.

We next present a similar LES of a S-shape duct but the concave-convex wall ($N/D_h = 0$) is now heated by imposing a temperature higher than the one of the other three walls with $T_h/T_w = 2$. The figure 12 shows that, at the duct outlet, the two vortices which can be observed close to the lower wall $n/D_h = 0.1$ are enhanced in size and intensity. We have checked that the mean longitudinal velocity profiles show that a flow acceleration coming from the extension of the thermal boundary layer near concave/convex wall.

In the first part of the duct, figure 11 shows a very abrupt temperature gradient near the heated wall. The very strong pressure gradient normal to the walls retains the hot fluid close to the heated wall. Further downstream, secondary vortices which form near the lower wall after the second bend (see figure 12) allows for an efficient transport of the hot fluid from the heated wall to the duct core. The T_{rms} profiles confirm that the extension of the mixing region is much larger close the second part of the duct. In observing the turbulent kinetic energy k and the Reynolds shear stress $\langle u'v' \rangle$, we remark that the values are shifted up in the heated case in the second part of the duct. The turbulence activity seems to be moved away from the hot wall.

In addition we can say that friction and pressure coefficients are smaller when heating is applied (see figure 10) excepted for the skin friction on the hot wall. The enhancement of viscosity of the fluid is probably responsible of the decreasing of the pressure coefficient.

CONCLUSIONS

In this study we tried to show the influence of the heat and of a curvature on a turbulent flow. The results were obtained by a LES simulation with a spatial evolution of the flow. This realistic conditions allowed us to understand developement of turbulent structures. Our new results concerning straight heated duct confirms that a spatial evolution is able to reproduce Salinas-Vasquez and Metais' simulations (2001) for a infinite duct in the longitudinal direction. The use of curvilinear coordinates allowed us to simulate a S-shape duct with and without heating and to understand the destabilizing effects of both concave walls. A first conclusion was the centrifugal forces change the turbulent structures and the normal pressure gradients move them. The turbulence intensities are enhanced near concave walls and decreased close to convex ones. The enhancement of the viscosity when heating is applied changes skin friction and pressure coefficient and shifts up turbulent intensities profiles. The same spatial configuration should be used for a heating which evolves in the longitudinal direction.

ACKNOWLEDGMENTS

All the numerical computations were carried out at the "Institut du Développement et des Ressources en Informatique Scientifique".

REFERENCES

Bruns J. M., Fernholz H. H. & Monkewitz P.A., 1999 "An experimental investigation of a three-dimensional turbulent boundary layer in an 'S'-shaped duct." *Journal of Fluid Mechanics*, Vol. 393, pp. 175-213.

Chebbi B., Holloway G.L. & Tavoularis S., 1998, "The response of sheared turbulence to changes in curvature", *Journal of Fluid Mechanics*, Vol. 358, pp. 223-244.

Dubief Y. & Delcayre F., 2000, "On coherent-vortex identification in turbulence .", *Journal of Turbulence*, Vol. 1.

Hunt J., Wray A., Moin P., 1988, "Eddies, stream, and convergence zones in turbulent flows." *Center for Turbulence Research Rep.*, Technical Report CTR-S88.

Jongen T., Mompean G. & Gatski T. B., 1998 "Predicting S-duct flow using a composite algebraic stress model." *AIAA Journal*, Vol. 36, pp. 327-335.

Kennedy C. A. & Carpenter M. H., 1997, "Comparison of several numerical Methods for simulations of compressible shear layers.", *NASA*, Paper 3384.

Lesieur M. & Métais O., 1996, "New trends in Large-eddy simulation of turbulence ", *Ann. Rev. Fluid Mech.*, Vol. 28, pp.45-82

Poinsot T. & Lele S., 1992, "Boundary conditions for direct simulations of compressible viscous flows.", *Journal of Computational Fluid*, Vol. 101, pp.104-129.

Salinas-Vasquez M. & Métais O., 2001, "Large-eddy simulation of a spatially growing thermal boundary layer i n a turbulent square duct", *Direct and Large-Eddy Simulation IV*

Salinas-Vasquez M. & Métais O., 2002, "Large-eddy simulation of the turbulent flow through a heated square duct", *Journal of Fluid Mechanics*, Vol. 453, pp. 201-238.